INTERNATIONAL JOURNAL FOR NUMERICAL METHODS IN FLUIDS
Int. J. Numer. Meth. Fluids 2008; **58**:1135–1146
Published online 20 March 2008 in Wiley InterScience (www.interscience.wiley.com). DOI: 10.1002/fld.1791

Simulating hydrostatic and non-hydrostatic oceanic flows

M. Iskandarani*, †

Rosenstiel School of Marine and Atmospheric Science, University of Miami, 4600 Rickenbacker Causeway, Miami, FL 33149, U.S.A.

SUMMARY

The thin aspect ratio of oceanic basins is simultaneously a complication to contend with when developing ocean models and an opportunity to simplify the equations of motion. Here we discuss these two aspects of this geometric feature in the context of hydrostatic and non-hydrostatic ocean models. A simple analysis shows that the horizontal viscous operator in the hydrostatic primitive equations plays a central role in the specification of boundary conditions on the lateral vertical surfaces bounding the domain. The asymptotic analysis shows that for very thin aspect ratios the leading-order flow cannot be closed unless additional terms in the equations are considered, namely either the horizontal viscous forces or the non-hydrostatic pressure forces. In either case, narrow boundary layers must be resolved in order to close the circulation properly. The computational cost increases substantially when non-hydrostatic effects are taken into account. Copyright © 2008 John Wiley & Sons, Ltd.

Received 18 April 2007; Revised 14 January 2008; Accepted 4 February 2008

KEY WORDS: hydrostatic Navier–Stokes; spectral element; permissible boundary conditions

1. INTRODUCTION

Oceanic flows are distinguished by the large disparities between the horizontal and vertical scales of motion. This is in large part due to the large aspect ratio of the ocean basin itself whose depth-to-width ratio, r, is very small. This length scale disparity is simultaneously an opportunity for model developers to construct efficient approximation to the Navier–Stokes equations and a source of computational challenges, particularly when one is interested in processes whose length scale is small compared with a typical basin dimension. Examples of the latter include small-scale mixing processes occurring over a sizable extant of ocean area.

*Correspondence to: M. Iskandarani, Rosenstiel School of Marine and Atmospheric Science, University of Miami, 4600 Rickenbacker Causeway, Miami, FL 33149, U.S.A.
†E-mail: miskandarani@rsmas.miami.edu

Contract/grant sponsor: National Science Foundation; contract/grant numbers: CNS0540155, OCE-0622662
Contract/grant sponsor: Office of Naval Research; contract/grant number: N000140510325

The equations governing oceanic flows are the incompressible and Boussinesq Navier–Stokes equations

$$\frac{\mathrm{d}\mathbf{u}}{\mathrm{d}t}+\mathbf{f}\times\mathbf{u}+g\nabla\eta+\frac{\nabla p}{\rho_0}=-g\frac{\rho}{\rho_0}\mathbf{k}+\nu_\mathrm{h}\nabla^2\mathbf{u}+\nu\mathbf{u}_{zz} \tag{1}$$

$$\nabla\cdot\mathbf{u}+w_z=0 \tag{2}$$

$$\frac{\mathrm{d}\rho}{\mathrm{d}t}=\kappa_\mathrm{h}\nabla^2\rho+\kappa\rho_{zz} \tag{3}$$

where $\mathbf{u}$ is the velocity, η the free-surface height; p the non-hydrostatic pressure; g the gravitational acceleration; $\mathbf{f}$ the Coriolis parameter; ρ a density anomaly considered small with respect to the reference density ρ_0; ν_h and ν the horizontal and vertical viscous coefficients, and κ_h and κ the diffusivity coefficients. For flows where the velocity scale U, and where the horizontal length scale L, is much larger than the vertical length scale D, the scaling of the continuity equation shows that the vertical velocity scales as $O(UD/L)$, with the results that the vertical momentum equation reduces to a simple hydrostatic balance counteracting the buoyancy force. The resulting hydrostatic equations are computationally advantageous as one does not need to invert an elliptic equation for the non-hydrostatic pressure.

The computational advantages of the hydrostatic approximation are accompanied by disadvantages. These are mostly of a mathematical nature, and include in particular the need to compute the vertical velocity diagnostically from the continuity equation. The vertical velocity takes on the role traditionally associated with the non-hydrostatic pressure in enforcing the continuity equation. As the latter contains no damping term, the vertical velocity inherits the noise in the divergence of the horizontal velocity components; the undamped vertical velocity reduces the mathematical regularity of the solution and complicates the mathematical analysis of the hydrostatic primitive equations (HPEs) substantially [1].

Another consequence of the hydrostatic approximation is concerned with the permissible boundary conditions on the lateral (vertical) boundaries. It is well known, for example, that the inviscid hydrostatic equations for the open-boundary problem are ill-posed for any *local* set of boundary conditions [2], whereas the viscous equations are well-posed [1]. Well-posedness can be recovered if one is willing to consider non-local boundary conditions as shown in Blayo and Debreu [3] and Rousseau *et al.* [4, 5]. The lack of regularity motivated Temam and Tribbia [6] and Rousseau *et al.* [4, 7] to propose a new set of equations where an additional damping term is introduced in the vertical momentum equation (the dynamical balance becomes non-hydrostatic even without reverting to the full Navier–Stokes equations). These modified equations lead to the formation of boundary layers as shown in Rousseau *et al.* [7].

The problems discussed here are concerned with the consequences of adopting or circumventing the hydrostatic approximation and the impacts of these choices on the simulation of oceanic flows. In particular, we present a curious limit of the hydrostatic equations where an asymptotic analysis in terms of the oceanic aspect ratio r shows that narrow viscous boundary layers are needed to close the recirculation associated with the normal flow at a boundary. The width of these recirculation zones is proportional to $r\sqrt{\nu_\mathrm{h}/\nu}$ for $\nu_\mathrm{h}/\nu\sim 1$, where ν_h and ν are the horizontal and vertical viscous coefficients, respectively; the recirculation zone is wider if $\nu_\mathrm{h}/\nu\sim r^{-1/2}$. In either case, it turns out that viscous effects are the sole actors in forming the recirculation zones within the basin. An alternative process is to include non-hydrostatic effects in the equations to form the recirculation

DOI: 10.1002/fld

zone; unfortunately, our analysis shows that their width also scales similar to r and hence remains within the subgrid scale of current ocean models. Although the latter ensures convergence to the right physics as the grid is refined, the computational burden associated with it is substantial, particularly when considering flows over large oceanic domains. This is illustrated by applying a non-hydrostatic model to simulate the mixing within a lock exchange problem, an idealized version of the gravity currents occurring in nature.

We emphasize that the viscous recirculation zones are needed to enforce the normal flow boundary conditions, and not the tangential velocity components, i.e. the no-slip condition, associated with the bottom Ekman layer, for example. The latter is usually associated with viscous effects, whereas the former is associated with pressure forces. It is also important to note that the narrow recirculation zones have no signature in the depth-average flow; this is a reflection of the fact that the shallow water equations form a set of well-posed equations, whereas the hydrostatic equations do not.

The article is structured as follows. Section 2 presents the linearized equations and its non-dimensional form. Section 2.1 discusses the solution to the inviscid equations and presents numerical results in support of the findings. Two alternatives are discussed to close the circulation by either introducing a horizontal viscous term, Section 2.2, or a non-hydrostatic pressure term, Section 2.3. The last section illustrates the computational burdens associated with including the non-hydrostatic pressure in the simulation. The latter must be included to produce the instabilities that cause the mixing.

2. THE HYDROSTATIC LINEARIZED PE EQUATIONS

Here we discuss a curious limit of the linear steady-state hydrostatic equation whereby the asymptotic analysis of the linearized equations produces a surprising singular perturbation problem, and where viscous boundary layers are required near the sidewall to bring the *normal* flow to zero. The discussion hence concerns primarily the dynamical balance on the lateral boundaries of the domain and touches on the issue of the admissible boundary conditions for the hydrostatic equations. The problem considered consists of studying the linear, steady-state circulation in a well-mixed, wind-driven flow in a rectangular basin of constant depth.

To simplify the analysis we will make several approximations:

1. The Coriolis force will be omitted even though it is one of the major terms in the momentum equations when considering motions whose timescale is longer than a rotation period. The Coriolis term, however, does not play a major role in determining the mathematical character of the equations and has no effect on the permissible boundary conditions. This will also allow us to consider the two-dimensional equations (x–z only).
2. Here we will be primarily concerned with the unstratified limit to simplify the algebra, hence setting $\rho = 0$. Stratification's impact on the momentum equation is via the baroclinic pressure gradient, a term that could be regarded as a forcing term for the velocity equation; its presence should not alter the nature of the permissible boundary conditions on the velocity.
3. Finally, in the absence of stratification, the eddy viscous coefficient, ν, could be considered isotropic in the horizontal and vertical directions as an unstratified fluid does not exhibit a preferred mixing direction. Hence, the viscosity ratio will be taken as $\varepsilon^2 = \nu_h/\nu = 1$.

DOI: 10.1002/fld

Using D and L as the vertical and horizontal length scales, respectively, T as the time scale and U as the horizontal velocity scale, we obtain the following equations:

$$u_t+\eta_x=[\alpha^2 u_{xx}+u_{zz}] \tag{4}$$

$$u_x+w_z=0 \tag{5}$$

The circulation is forced by a unit wind-stress applied uniformly at the surface. The non-dimensional linearized free surface and bottom boundary conditions are

$$vu_z=1 \quad \text{and} \quad \eta_t=\frac{gD}{L^2}\left(\frac{D}{v}\right)^2 w \ \text{ at } z=0 \tag{6}$$

$$\gamma^{-1}u_z=u \quad \text{and} \quad w=0 \ \text{ at } z=-1 \tag{7}$$

where we have used the same notation for the dimensional and non-dimensional variables. Here we have set the timescale to $T=D^2/v$, the vertical velocity scale to $W=UD/L$, the horizontal velocity scale to $U=D|\tau|/\rho v$ (τ is the surface wind-stress), and the surface displacement scale to $a=vLU/(gD^2)=|\tau|L/(\rho gD)$. Lastly, the non-dimensional horizontal viscosity is $\alpha^2=r^2$, where $r=D/L$ is the aspect ratio. A bottom stress law is applied on the seabed with a bottom drag coefficient of γ; the no-slip case corresponds to $\gamma^{-1}\to 0$.

2.1. *Two-dimensional horizontal inviscid flow*

In this first instance, we solve the problem in the limit $\alpha\to 0$; the steady-state equations become

$$\eta_x=u_{zz}, \quad u_z|_{z=0}=1, \quad \gamma^{-1}u_z|_{z=-1}=u(x,-1) \tag{8}$$

$$u_x+w_z=0, \quad w(x,0)=0, \quad w(x,-1)=0 \tag{9}$$

2.1.1. Theoretical analysis. As η_x is depth independent, we can integrate the momentum equation (8) in the vertical to obtain the horizontal velocity component and its associated vertical velocity:

$$u=\frac{\eta_x}{2}(z^2-1)+(z+1)+\gamma^{-1}(1-\eta_x) \tag{10}$$

$$w=-\eta_{xx}\left[\frac{z^3}{6}-z\left(\frac{1}{2}+\gamma^{-1}\right)\right] \tag{11}$$

The above expressions take into account the surface stress and bottom drag boundary conditions on u and the surface condition on w; the surface slope η_x is still undetermined. The vertical velocity at the seabed is $w=-\eta_{xx}(\gamma^{-1}+\frac{1}{3})$ so that the surface condition can be satisfied (for arbitrary γ) only if $\eta_{xx}=0$. The free surface must then have constant slope and the vertical velocity must be zero everywhere. The continuity equation (11) requires the horizontal velocity to be uniform in the x-direction; one cannot impose a no-throughflow boundary condition as it would imply the flow to be zero everywhere. The slope η_x can be determined by imposing the horizontal transport to obtain

$$\eta_x=\frac{3}{2}\frac{1+2\gamma^{-1}-2\mathscr{U}}{1+3\gamma^{-1}}, \quad \mathscr{U}=\int_{-1}^{0} u\,\mathrm{d}z \tag{12}$$

Note that the transport condition is a depth-integrated condition devoid of z-dependency.

DOI: 10.1002/fld

2.1.2. Numerical experiments. To confirm these analytical findings we have conducted numerical experiments using the spectral element ocean model (SEOM). The SEOM formulation is an extension of Galerkin low-order, finite element methods; it uses hexahedral elements and high-order interpolation for spatial discretization. The key aspect of SEOM for this discussion is that its high-order spatial representation is highly accurate and inviscid. Details of the SEOM algorithms may be found in [8].

With steady wind forcing, and linear bottom drag as described in the prior section, we have run SEOM to steady state in several configurations. The basic setup is a $3\times3\times1$ elemental discretization in the $x\times y\times z$ directions, respectively, using sixth-order (third-order) velocity interpolation in the horizontal (vertical) direction. This is sufficient to recover the parabolic vertical structure of the solution. We have set $\gamma=1$ for this set of numerical experiments.

The first experiment attempts to reach steady state while imposing a no-throughflow boundary condition at $x=0,1$. The free surface undulates before straightening out and reaching its expected steady-state linear slope. The implied slope as measured by the SEOM data is $\eta_x=1.125000=\frac{9}{8}$, exactly as predicted by Equation (12). The bottom and surface velocities are given by $u(0)=0.31250$ and $u(-1)=-0.12500$, respectively. The results indicate that SEOM predicts the correct solution for the horizontal velocity and surface velocity shapes. Nonetheless, errors arise in the vertical velocity field, shown in Figure 1, which is non-zero and which oscillates in the x-direction. The vertical velocity vanishes in the middle element, $|w|=O(10^{-7})$, and displays steep boundary layers near the edges. These layers are an artifact of enforcing a non-admissible boundary condition on u. The non-uniformity in u creates a spurious divergence and leads to an unphysical vertical velocity.

The second experiment consists of applying no boundary conditions on u whatsoever. The solution behaves exactly as predicted by the analysis, reproducing a horizontally uniform u (including the lateral boundaries) that varies quadratically in the vertical, and a very small vertical velocity accompanied by a linear slope of the free surface. The plots are omitted as they are indistinguishable from those shown in Figure 1, except that now $|w|\sim O(10^{-7})$ everywhere.

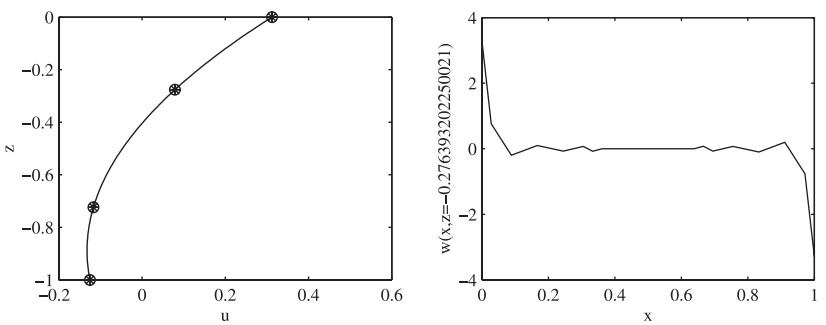

Figure 1. Numerical experiment imposing the no-through boundary condition at $x=0,1$. Left panel: $u(x=\frac{1}{2},z)$ (the results are uniform in x), the symbols are the SEOM results and the solid line is the analytical solution. Right panel: horizontal profile of w at the first computational level below the free surface. The vertical velocity in the interior of the middle element is very small ($O(10^{-7})$). The oscillations in the boundary elements are due to the spurious lateral boundary condition on u.

DOI: 10.1002/fld

The analysis in this section shows that, in the absence of additional physics, local lateral boundary conditions on u cannot be imposed. What can be imposed is the transport that involves non-local data. These results are in agreement with those presented in Temam and Tribbia [6] for a stratified atmospheric case, and with those of Rousseau *et al.* [4] concerning the non-locality of the permissible boundary conditions. If the boundary is closed, and the flow cannot exit the basin, the recirculation has to take place via infinitesimally small upwelling/downwelling regions at the lateral boundaries; these regions would be one cell wide in a numerical model.

2.2. *Two-dimensional horizontal viscous flow*

Clearly, an additional physical mechanism is needed to impose the vertical structure of the flow at the lateral boundary and to render the problem well-posed. In this section, we explore the implication of admitting horizontal viscous forces. We thus retain the horizontal viscous term $\alpha^2 u_{xx}$ in Equation (8). As homogeneous Dirichlet conditions are imposed at both ends of the domain, it is reasonable to expand the solution in sine and cosine series and obtain the analytical solution by separation of variables.

2.2.1. Asymptotic analysis. It is, however, more instructive to consider the asymptotic solution for $\alpha \ll 1$. To simplify the analysis, we differentiate the viscous version of the momentum equation in the vertical to derive an equation for the vertical shear

$$\alpha^2 u_{zxx} + u_{zzz} = 0 \tag{13}$$

In the interior, where horizontal viscous forces can be neglected, the solution proceeds as in the previous section and is given by Equations (10)–(12). In the following we will refer to it with the superscript i. Near the sidewalls a boundary layer is required to counteract the vertical shear and bring the normal flow to a halt. We thus introduce the scaled coordinate $\xi = x/\alpha$, define the boundary layer velocity $u^{(b)} = u - u^{(i)}$, and substitute into the momentum equation and boundary conditions to derive the governing equations for $u_z^{(b)}$

$$u^{(b)}_{z\xi\xi} + u^{(b)}_{zzz} = 0, \quad u^{(b)}_z|_{z=0} = 0, \quad u^{(b)}_z|_{z=-1} = \gamma u^{(b)}|_{z=-1} \tag{14}$$

Additional lateral boundary conditions are needed to fully specify the problem; we impose the conditions of no-flow on the solid walls, $u^{(b)}(0, z) = -u^{(i)}(z)$, and that the boundary layer flow vanishes far from the wall, $u^{(b)}(\xi \to \infty, z) = 0$. The boundary layer solution is given by

$$u^{(b)}(\xi, z) = \sum_{n=1}^{\infty} D_n \mathrm{e}^{-\lambda_n \xi} \cos \lambda_n z, \quad \lambda_n \tan \lambda_n = \gamma, \quad D_n = \frac{4\lambda_n}{2\lambda_n + \sin 2\lambda_n} \int_{-1}^{0} u^{(i)}(z) \cos \lambda_n z \, \mathrm{d}z \tag{15}$$

The x-dependence of the boundary layer solution consists of an infinite number of exponentially decaying modes with a decay length scale of $O(\alpha \lambda_n^{-1})$, where λ_n refers to the vertical eigenvalues. As eigenvalues increase with n, the decay length of each mode decreases linearly. The modal amplitudes D_n depend on the vertical structure of the interior flow.

2.2.2. Viscous simulations. The numerical solution in the presence of horizontal viscosity is shown in Figure 2. We have enforced the boundary condition $u = 0$ at both ends of the domain. This small value of viscosity leads to the formation of boundary layers for u near the lateral walls. Their estimated width according to the previous analysis is 0.05 and 0.03 for the first and second modes,

DOI: 10.1002/fld

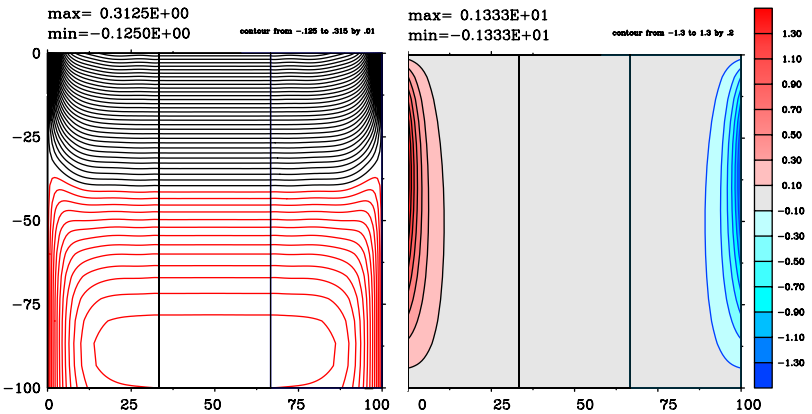

Figure 2. Velocity components in the presence of horizontal viscosity $\alpha^2 = 0.03$. The left and right panels show the u and w contours, respectively.

respectively. The SEOM grid has only two points within these boundary layers. Note also that the vertical contours show no Gibbs oscillations: lateral viscous action has inflated the width of the recirculation zone from 0 to something that can be represented on a discrete grid.

The viscous case shown here confirms portions of the asymptotic analysis. The flow remains predominately uniform in the interior and has a vertical parabolic structure. Rapid changes take place near the lateral walls to bring the flow to a halt throughout the water column. The lesson for hydrostatic ocean models is that the flow structure near the boundary is dominated by (explicit or numerically induced) viscous forces. An alternative modification to the hydrostatic equations that does permit the imposition of local boundary conditions is the inclusion of a dissipation term in the vertical momentum equation as suggested by Temam and Tribbia [6]; interestingly, for small dissipation this solution also leads to lateral boundary layers that were analyzed in Rousseau *et al.* [7].

2.3. *Non-hydrostatic flows*

Another physical mechanism that can bring the normal flow to rest is the non-hydrostatic pressure. Here we attempt to estimate the width of the non-hydrostatic boundary layer needed to close the circulation. The steady-state, non-rotating, and non-dimensional form of the non-hydrostatic momentum equations for a homogeneous density fluid is

$$\eta_x + r p_x = \alpha^2 u_{xx} + u_{zz} \tag{16}$$

$$p_z = \alpha^2 r w_{xx} + r w_{zz} \tag{17}$$

where p is the non-hydrostatic normalized pressure ($p = p^*/|\tau|$, where p^* is the dimensional pressure), and $r = D/L$ is the aspect ratio of the domain.

2.3.1. Theoretical analysis. The system can be recast into a vorticity equation

$$\alpha^2 (r^2 \psi_{xx} + \psi_{zz})_{xx} + (r^2 \psi_{xx} + \psi_{zz})_{zz} = 0 \tag{18}$$

DOI: 10.1002/fld

with the streamfunction, and vorticity defined as $u=\psi_z$, $w=-\psi_x$, and $\zeta=-r^2\psi_{xx}+\psi_{zz}$, and where $\alpha=\varepsilon r$. We have retained the horizontal viscous term in the vorticity equation (18) because of the quadratic factor in r. The appropriate asymptotic form depends on the two parameters $r=D/L$ and $\varepsilon^2=\nu_h/\nu$. For the case where $\varepsilon\sim O(1)$ and $\alpha\sim O(r)\ll 1$, non-hydrostatic effects and horizontal viscous forces enter into play simultaneously as the vorticity equation receives equal contributions from the horizontal viscous forces, $\alpha^2\psi_{zzxx}$, in the first bracketed term (the horizontal diffusion of the vertical portion of vorticity: $-\alpha^2(u_z)_{xx}$), and non-hydrostatic effect, $r^2\psi_{xxzz}$, in the second bracketed term (vertical diffusion of the non-hydrostatic portion of vorticity: $(r^2w_x)_{zz}$).

The boundary conditions on the top and lower surfaces are

$$\psi(x,0)=\psi(x,-1)=0,\quad \psi_z(x,0)=1,\ \ \psi_{zz}=\gamma\psi_z \text{ at } z=-1 \tag{19}$$

where we have already assumed a zero net transport in the water column. The lateral boundary conditions for a closed domain must be $\psi(0,z)=\psi(1,z)=0$ plus additional boundary conditions involving the vertical velocity. The latter can be either no-slip $\psi_x=0$ or free slip $\psi_{xx}=0$ at $x=0,1$. The biharmonic equation (18) can now be fully solved, and all boundary conditions can be applied.

Note that hydrostatic effects alone are enough to allow prescription of the normal flow at the lateral boundary. The (unjustified) neglect of the first term in Equation (18) would yield

$$(r^2\psi_{xx}+\psi_{zz})_{zz}=0 \tag{20}$$

which is a second-order equation in x and fourth order in z; thus two lateral boundary conditions on x (one on each side) and four boundary conditions on the horizontal boundaries (two at the top and two at the bottom) can be applied. One can easily anticipate that the boundary layer through which the streamfunction must change to enforce the lateral boundary condition must be $\sim O(r)$. The inclusion of the horizontal diffusion of vorticity does not change that scaling.

2.3.2. Non-hydrostatic simulations. Here we solve the non-hydrostatic case in vorticity–streamfunction form. The equations being solved are

$$r^2\zeta_{xx}+\zeta_{zz}=0 \tag{21}$$

$$r^2\psi_{xx}+\psi_{zz}+\zeta=0 \tag{22}$$

with boundary conditions: (1) $\psi=0$ around the entire boundary; (2) $\zeta(x,0)=w_x-u_z=1$ on the surface; (3) no-slip boundary conditions on the bottom; and (4) in order not to deal with the vertical velocity at the intersection of a solid wall and moving free surface, free-slip boundary conditions on the vorticity at the lateral walls: $\zeta(0,z)=\zeta(1,z)=0$. Note that vorticity is discontinuous at the corners where the lateral walls meet the free surface. The spectral element grid was thus redesigned with these issues in mind, and we have used six spectral elements in the horizontal and four in the vertical with spectral truncation 7. The element sizes in the horizontal are 0.1, 0.15, 0.25, 0.25, 0.15, 0.1 and in the vertical are 0.1, 0.4, 0.4, and 0.1, respectively.

Two cases were run for $r=0.1$ and 0.01. The along-wind velocity is shown in Figure 3. The solution that emerges tells the same story as before, producing a horizontally uniform flow with no-vertical motion (as evidenced by the flat streamlines) and a rapidly varying solution near the boundary. The width of the boundary layer is $O(r)$ in both instances. Note that the solution for

DOI: 10.1002/fld

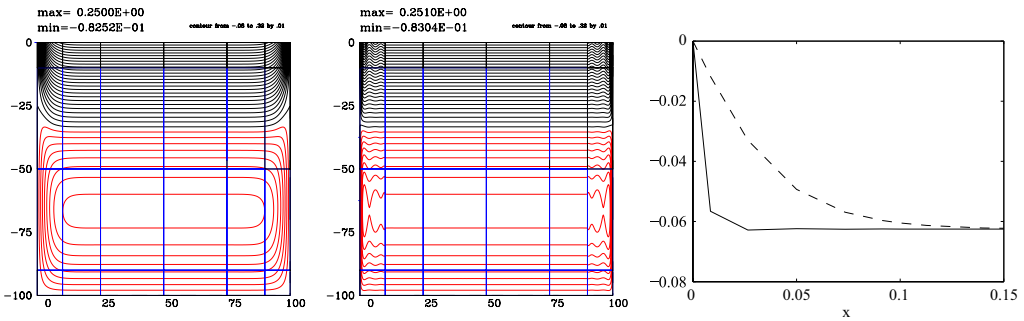

Figure 3. Contours of u for $\alpha = r = 0.1$ (left) and $\alpha = r = 0.01$. The right panel shows a horizontal section of u in the boundary layer at a depth $z = -0.5$; the dashed and solid lines correspond to $r = 0.1$ and 0.01, respectively.

$r = 0.01$ exhibits oscillations, tell-tale signs of an under-resolved simulation. Figure 3 shows a horizontal section of u and ζ at mid-depth; it confirms the $O(r)$ scaling of the boundary-layer width and the uniformity of the flow in the interior.

The presence of bathymetric variation should also not change the nature of the boundary conditions one can apply on the lateral sides. It does, however, lead to important changes in the nature of the interior flow as it leads to vertical motion away from the boundary.

3. NON-HYDROSTATIC MIXING IN GRAVITY CURRENTS

Although the hydrostatic approximation is valid for a wide range of oceanic flow regimes, it fails to be valid in some important flows where vertical accelerations are critical. One example is the mixing due to gravity currents emanating from marginal seas, such as the dense Mediterranean water flowing into Atlantic Ocean at Gibraltar Strait, or the Red Sea outflow at Bab-El-Mandab into the Indian Ocean. In these cases, the computational challenges consist in representing small-scale mixing dynamics O(tens of meters) spanning large flow regions.

To illustrate the numerical challenges, we consider the non-dimensional Boussinesq Navier–Stokes equations in their streamfunction–vorticity form

$$\zeta_t + \mathbf{u}\cdot\nabla\zeta = \frac{1}{Re}\nabla^2\zeta - \frac{1}{Fr^2}\rho_x, \quad Re = \frac{UL}{\nu}, \quad Fr = U\left(g\frac{\Delta\rho}{\rho_0}L\right)^{-1/2} \tag{23}$$

$$\nabla^2\psi + \zeta = 0 \tag{24}$$

$$\rho_t + \mathbf{u}\cdot\nabla\rho = \frac{1}{PrRe}\nabla^2\rho, \quad Pr = \frac{\nu_\rho}{\nu} \tag{25}$$

where ρ is the non-dimensional density *anomaly* and the non-dimensional numbers are the Reynolds number Re, the Froude number Fr, and the Prandtl number Pr, which is the ratio of density diffusion to viscous dissipation. The fluid velocity is given by $\mathbf{u} = (\psi_y, -\psi_x)$.

DOI: 10.1002/fld

The classical conforming weak formulations [9] of the Poisson and vorticity equations are

$$\int_A \zeta_t \phi \, \mathrm{d}A = \int_A \left[\left(\zeta \mathbf{u} - \frac{\nabla \zeta}{Re} \right) \cdot \nabla \phi + \mathbf{f} \times \nabla \phi \right] \mathrm{d}A + \int_{\partial A} \phi \left[\left(-\zeta \mathbf{u} + \frac{\nabla \zeta}{Re} \right) \cdot \mathbf{n} + \mathbf{n} \times \mathbf{f} \right] \mathrm{d}S \tag{26}$$

$$\int_A \nabla \psi \cdot \nabla \Psi \, \mathrm{d}A = \int_A \zeta \Psi \, \mathrm{d}A \tag{27}$$

where the buoyancy force is $\mathbf{f} = (0, -\rho/Fr^2)$. The density evolution equation is essentially an advection–diffusion equation at very high Peclet number. There are well-known difficulties in solving these equations in the advection-dominated regime using centered-type schemes such as spectral elements. Discontinuous Galerkin methods (DGMs) [10] are much more suitable, especially when fronts may be present. The density evolution equation in the DGM form is

$$\int_{A_e} \chi \frac{\partial \rho}{\partial t} \, \mathrm{d}A = \int_{A_e} \left(\mathbf{u}\rho - \frac{\mathbf{q}}{PrRe} \right) \cdot \nabla \chi \, \mathrm{d}A + \int_{\partial A_e} \left(\mathbf{u}\tilde{\rho} + \frac{1}{PrRe} \tilde{\mathbf{q}} \right) \cdot \mathbf{n} \chi \, \mathrm{d}S \tag{28}$$

$$\int_{A_e} \Phi \mathbf{q} \, \mathrm{d}A = \int_{\partial A_e} \Phi \tilde{T} \mathbf{n} \, \mathrm{d}S - \int_{A_e} T \nabla \Phi \, \mathrm{d}A \tag{29}$$

where χ are the *discontinuous* shape and weight functions, $\tilde{\rho}$ refers to the density taken from the upstream of edges ∂A_e, and $\mathbf{q}$ refers to the diffusive fluxes computed as the weak gradient of the function T. Shu [11] discusses different formulations for the diffusive and advocates alternating the exchange directions between those of the element and those of its neighbor. Thus, if $\tilde{T} = T^-$ then $\tilde{\mathbf{q}} = \mathbf{q}^+$, where the superscripts $-$ and $+$ refer to values interior and exterior to an element, respectively. The Galerkin discretization proceeds by dividing the flow domain into quadrilateral spectral element and representing the solution in terms of Lagrangian polynomials. We skip the details and refer the reader to Karniadakis and Sherwin [12] and Deville *et al.* [9] for more information.

The following points are worth mentioning regarding the discretization and integration procedures. First, the vorticity equation is integrated explicitly using a third-order Adams–Bashforth scheme, and all interior vorticity values are updated. Second, the streamfunction is updated by solving Equation (27). A substructing scheme is used to consolidate the system of equations into the degrees of freedom on the edges of elements, and the latter system is solved with conjugate gradient iterations using diagonal preconditioning. The procedure suggested by Liu and Weinan [13, 14] can be used if no-slip boundary conditions need to be applied. Third, the density field is time integrated using an AB3 scheme.

The numerical model was applied to study the lock exchange problem of a two-density fluid in a rectangular domain with a 5×1 aspect ratio (this is still far from the realistic case where it could reach 100×1). The Reynolds number was set to $Re = 10\,000$, the Froude number to 2, and the Prandtl number to 7. The spatial discretization was effected with a 128×25 spectral elements of degree 14 for the streamfunction and vorticity, and of degree 13 for the density. The domain was closed on all sides and free-slip boundary conditions were applied (the focus is on the interfacial mixing between the two layers). Figure 4 shows a snapshot of density contours depicting the vigorous mixing between the two fluids. The low dissipation and accurate representation afforded by the spectral element discretization are evident in the sharp interfaces between the various density regions. Nevertheless, tiny spots of small over ($\rho > 1$) and undershoots ($\rho < 0$) of the density fields can be detected and are evidence of local and spotty under-resolution of the density fields.

DOI: 10.1002/fld

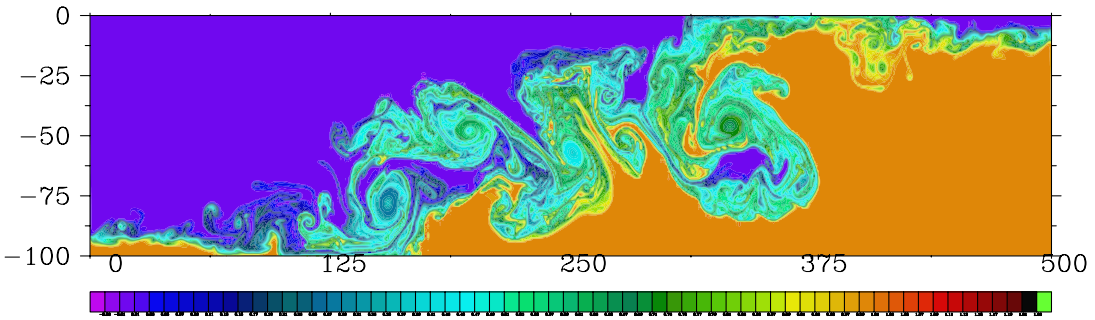

Figure 4. Density contours of a lock exchange problem using a spectral element discretization of the equations. The light fluid is indicated by blue color and the dense fluid is indicated by orange color. The density minimum is −0.0553 and the maximum is 1.0653. The density contours range from −0.03 to 1.22 by 0.02.

These oscillations are benign in the present case because their amplitudes are small (∼6% of original density contrast), and their extent is very limited. These oscillations can be eliminated by increasing the resolution globally or adaptively, or by adding dissipation via additional viscosity or via limiters (e.g. [15]). Increased resolution is the preferred recommendation as it avoids the introduction of numerical artifacts.

The computational challenges to model larger regions are staggering. In addition to using larger parallel computers, algorithmic development is needed, particularly for the efficient iterative solution to the Poisson equation.

4. DISCUSSION

The enforcement of the normal flow boundary conditions at lateral walls for the HPEs depends strongly on the horizontal viscous operator for the classical HPEs used commonly in ocean models. This is most clearly illustrated in the case of a wind-driven flow in an unstratified, non-rotating, and constant-depth rectangular basin. The interior flow is uniform horizontally, has a parabolic vertical profile, and cannot feel the presence of the lateral walls unless horizontal viscous effects are included in the equations. In that case, recirculation boundary layers appear, whose width is proportional to the aspect ratio of the basin and the square root of the horizontal-to-vertical viscosity ratio.

The development of a normal pressure gradient to slowdown the oncoming flow is prevented by the absence of such a mechanism in the hydrostatic equations. The tilt of the free surface provides a vertically uniform pressure gradient with no vertical structure to slowdown the oncoming flow; its effect is entirely felt by the depth-integrated flow. A three-dimensional pressure gradient can be formed only by the inclusion of non-hydrostatic effects. Then, our analysis shows that the width of the resulting boundary layers also scales similar to the aspect ratio of the basin and hence remains within the subgrid scale of most current ocean models.

The issues discussed here are a reflection of the fact that local boundary conditions cannot be imposed on the inviscid HPE equations as discussed in Oliger and Sundström [2] and Temam and Tribbia [6]. Alternative remedies not discussed here include the modification of the vertical

DOI: 10.1002/fld

momentum equation Temam and Tribbia [6] or imposing non-local boundary conditions of integral type [4].

Although our analysis has focussed thus far on lateral boundaries where a no-flow boundary condition is applied, the present results apply equally to all lateral boundaries where the vertical structure of the velocity is imposed. The most noteworthy case is that of the 'open' boundaries of nested models where velocity data, whether from observations or a more coarse larger-scale model, must be prescribed.

ACKNOWLEDGEMENTS

The author would like to acknowledge the support of the National Science Foundation (grants CNS0540155 and OCE-0622662) and the Office of Naval Research (grant N000140510325).

REFERENCES

1. Lions JL, Temam R, Wang S. On the equations of the large-scale ocean. *Nonlinearity* 1992; **5**:1007–1053.
2. Oliger J, Sundström A. Theoretical and practical aspects of some initial boundary value problems in fluid mechanics. *SIAM Journal on Applied Mathematics* 1978; **35**:419–446.
3. Blayo É, Debreu L. Revisiting open boundary conditions from the point of view of characteristic variables. *Ocean Modelling* 2005; **9**:231–252.
4. Rousseau A, Temam R, Tribbia J. Boundary conditions for the 2D linearized PEs of the ocean in the absence of viscosity. *Discrete and Continuous Dynamical Systems* 2005; **13**(5):1257–1276. ISSN 1078-0947.
5. Rousseau A, Temam R, Tribbia J. Numerical simulations of the inviscid primitive equations in a limited domain. In *Analysis and Simulation of Fluid Dynamics*, Calgaro C, Coulombel J-F, Goudon T. Advances in Mathematical Fluid Mechanics, Berkhaüser: Basel, 2007.
6. Temam R, Tribbia J. Open boundary conditions for the primitive and Boussinesq equations. *Journal of the Atmospheric Sciences* 2003; **60**(21):2647–2660.
7. Rousseau A, Temam R, Tribbia J. Boundary layers in an ocean related system. *Journal of Scientific Computing* 2004; **21**(3):405–432.
8. Haidvogel DB, Beckmann A. *Numerical Ocean Circulation Modeling*. Imperial College Press: London, U.K., 1999.
9. Deville MO, Fischer PF, Mund EH. *High-order Methods for Incompressible Fluid Flow*. Cambridge Monographs on Applied and Computational Mathematics. Cambridge University Press: Cambridge, U.K., 2002.
10. Cockburn B. An introduction to the discontinuous Galerkin method for convection dominated flows. In *Advanced Numerical Approximation of Nonlinear Hyperbolic Equations*, Quarteroni A (ed.). Springer: Berlin, 1998; 151–268.
11. Shu C-W. Different formulations of the discontinuous Galerkin method for the viscous term. In *Advances in Scientific Computing*, Shi Z-C, Mu M, Xue W, Zou J (eds). Science Press: Moscow, 2001; 144–155.
12. Karniadakis GEM, Sherwin SJ. *Spectral/hp Element Methods for CFD*. Oxford University Press: Oxford, 1999.
13. Weinan E, Liu J-G. Vorticity boundary conditions and related issues for finite difference schemes. *Journal of Computational Physics* 1996; **124**:368–382.
14. Liu J-G, Weinan E. Simple finite element method in vorticity formulation for incompressible flows. *Mathematics of Computation* 2000; **70**(234):579–593.
15. Burbeau A, Sagaut P, Bruneau Ch-H. A problem-independent limiter for high-order Runge–Kutta discontinuous Galerkin methods. *Journal of Computational Physics* 2001; **169**(1):111–150.

DOI: 10.1002/fld